

PCCP

Accepted Manuscript



This is an *Accepted Manuscript*, which has been through the Royal Society of Chemistry peer review process and has been accepted for publication.

Accepted Manuscripts are published online shortly after acceptance, before technical editing, formatting and proof reading. Using this free service, authors can make their results available to the community, in citable form, before we publish the edited article. We will replace this *Accepted Manuscript* with the edited and formatted *Advance Article* as soon as it is available.

You can find more information about *Accepted Manuscripts* in the [Information for Authors](#).

Please note that technical editing may introduce minor changes to the text and/or graphics, which may alter content. The journal's standard [Terms & Conditions](#) and the [Ethical guidelines](#) still apply. In no event shall the Royal Society of Chemistry be held responsible for any errors or omissions in this *Accepted Manuscript* or any consequences arising from the use of any information it contains.

Analysis of Transition State Stabilization by Non-Covalent Interactions in the Houk-List Model of Organocatalyzed Intermolecular Aldol Additions using Functional-Group Symmetry-Adapted Perturbation Theory

Brandon W. Bakr¹ and C. David Sherrill^{1,2, a)}

¹⁾*Center for Computational Molecular Science and Technology,
School of Chemistry and Biochemistry, Georgia Institute of Technology, Atlanta,
GA 30332-0400*

²⁾*School of Computational Science and Engineering, Georgia Institute of Technology,
Atlanta, GA 30332-0280*

(Dated: 21 March 2016)

Rational design of catalysts would be aided by a better understanding of how non-covalent interactions stabilize transition states. Here, we apply the newly-developed Functional-Group Symmetry-Adapted Perturbation Theory (F-SAPT) to quantify non-covalent interactions in transition states of the proline-catalyzed intermolecular aldol reaction between benzaldehyde and cyclohexanone, according to the Houk-List mechanism [Bahmanyar *et al.*, *J. Am. Chem. Soc.* 2003, **125**, 2475]. A recent re-examination of this organocatalytic reaction by Rzepa and co-workers [Armstrong *et al.*, *Chem. Sci.* 2014, **5**, 2057] used electron density analysis to identify three key non-covalent interactions thought to influence stereoselectivity: (1) a favorable electrostatic interaction (originally identified by Houk and List) between the $\text{NCH}^{\delta+}$ group of the enamine intermediate and the $\delta^- \text{O}=\text{C}$ of benzaldehyde; (2) a $\text{C-H}/\pi$ interaction between the cyclohexene group of the enamine intermediate and the benzaldehyde phenyl ring; (3) a stabilizing contact between an *ortho*-hydrogen of the phenyl and an oxygen of the carboxylic acid group of the enamine. These three interactions have been directly computed using F-SAPT, which confirms the stabilizing interaction between an *ortho*-hydrogen and the carboxylic acid in the (*S,S*) and (*R,S*) transition state stereoisomers. F-SAPT analysis also finds stabilizing dispersion and electrostatic interactions due to a $\text{C-H}/\pi$ interaction between the cyclohexene and phenyl groups in the (*S,S*) and (*R,R*) transition states. However, unfavorable exchange-repulsion cancels the attractive terms that favor these stereoisomers. Surprisingly, the interaction thought to be most important for stereoselectivity, the $\text{NCH}^{\delta+} \cdots \delta^- \text{O}=\text{C}$ interaction, is actually found to be repulsive due to the negative charge on the nitrogen. Hence, our results indicate that geometric analysis and/or density-based analysis does not necessarily produce a reliable picture of non-covalent stabilization. As confirmed by high-level coupled-cluster computations, intermolecular interaction energies are strongest for the (*R,R*) transition states, which are not the experimentally favored products. This suggests that at least for this reaction, stereoselectivity is also strongly dependent on the energy required to distort the reacting molecules into the transition state geometry.

^a)Electronic mail: sherrill@gatech.edu

I. INTRODUCTION

Catalytic design would benefit greatly from a more detailed understanding of the factors influencing transition state energetics. As recognized by the “distortion-interaction” model of Ess and Houk¹ and the “activation strain” model of Bickelhaupt and co-workers,² the two factors determining the energy of a transition state are (1) the strain energy required to deform the reactants into the transition state geometry, and (2) the stabilization coming from intermolecular interactions between the reactants. Indeed, a seminal paper by Houk, List, and co-workers³ proposes that non-covalent interactions (NCI) that stabilize transition states can determine the stereoselectivity of proline-catalyzed aldol reactions. Rzepa and co-workers⁴ have recently re-examined this reaction and claim that inspection of non-covalent interactions “is shown to be a useful tool for the design of alternative reactants.”

In their study, Rzepa and co-workers used the NCIPLOT program,⁵ which provides a 3D color-coded map based on the values of the density, the reduced density gradient, and the Laplacian of the density. Johnson et al.⁶ found an empirical correlation between various combinations of these quantities and the type and qualitative strength of NCI. Relying on this density-based analysis, Rzepa and co-workers identified additional sources of non-covalent stabilization of transition states in proline-catalyzed aldol reactions.

The density-based NCI analysis provides a simple and intuitive way to visualize intermolecular interactions. However, it does not provide energetics for these interactions. Symmetry-adapted perturbation theory (SAPT)^{7,8} does provide energetics for NCI, and it also provides the fundamental components of these interactions: electrostatics, induction/polarization, London dispersion forces, and steric exchange-repulsion. Such information is very helpful in understanding NCI,⁹ but for catalytic design, even more fine-grained information would be useful: one would also like to know the non-covalent stabilization or destabilization *between individual pairs of functional groups*. Fortunately, this information is now available through functional-group SAPT (F-SAPT), recently developed by our group.¹⁰

Here we apply F-SAPT to the proline-catalyzed aldol reaction in order to quantify the strength of the NCI proposed by Houk and co-workers³ and by Rzepa and co-workers⁴ as being important for transition state stabilization and stereoselectivity for the proline-catalyzed aldol reaction of benzaldehyde and cyclohexanone.

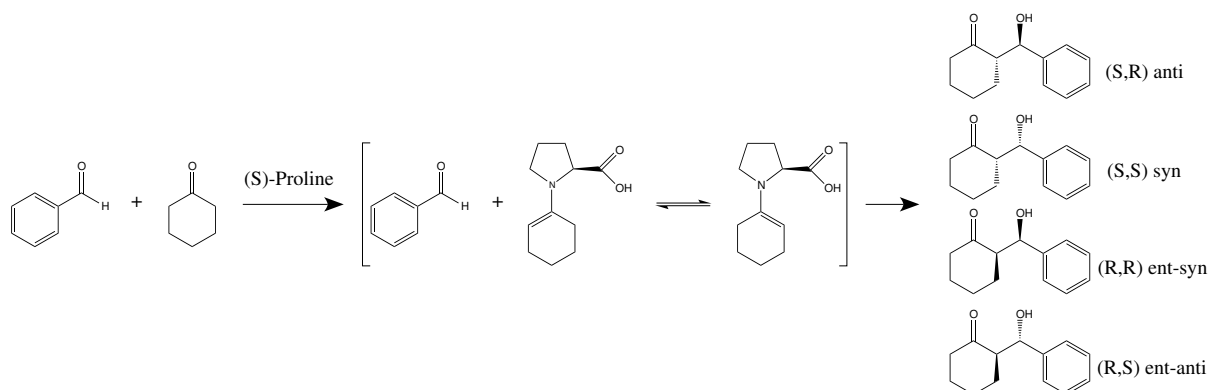


FIG. 1. The proline-catalyzed reaction between benzaldehyde and cyclohexanone along with the four possible stereochemical outcomes [(*S,R*) *anti*, (*S,S*) *syn*, (*R,R*) *ent-syn*, and (*R,S*) *ent-anti*]. Proline catalyzes the reaction by reacting with cyclohexanone to form a reactive enamine intermediate.

Four different stereoisomers can result from this reaction, as illustrated in Figure 1. The (*S,R*) *anti* and (*S,S*) *syn* products appear in near equal product ratios, 45-47% and 43-45% respectively.³ Likewise, the (*R,R*) *ent-syn* and (*R,S*) *ent-anti* stereoisomers have product ratios of 5-7% and 3-5% respectively.³ Four stereoisomers are possible because the carbon-carbon double bond that takes part in the C-C bond formation can exist on the same side or the opposite side of the carboxylic acid group in the enamine intermediate, and because the phenyl group of benzaldehyde can be oriented in two different ways relative to the enamine intermediate, as illustrated in Figure 2. Rzepa and co-workers⁴ have identified four low-lying conformers for each of these four families of transition states (see Figure 3), leading to a total of 16 relevant possible transition state structures.

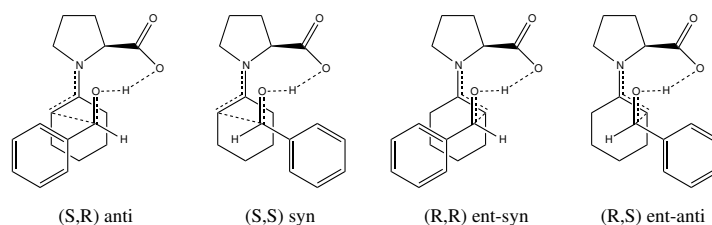


FIG. 2. Transition states, without specified conformations, leading to each possible stereoisomer [(*S,R*) *anti*, (*S,S*) *syn*, (*R,R*) *ent-syn*, and (*R,S*) *ent-anti*] of the product. The stereochemistry is determined by the relative orientations of the phenyl group of benzaldehyde and the forming carbon-carbon bond.

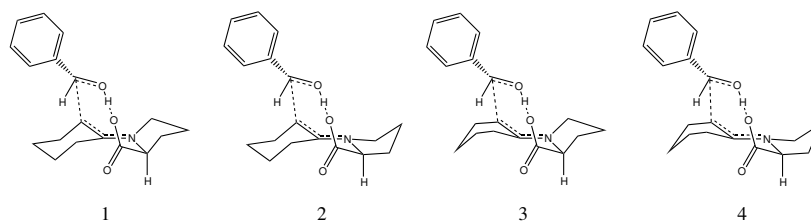


FIG. 3. The four low-lying conformations for each transition state stereoisomer. The pyrrolidinyllike ring is pucker away from benzaldehyde in conformers 1 and 3, and pucker towards it in conformers 2 and 4. Cyclohexene adopts a chair conformation in conformers 1 and 2, and a boat conformation in conformers 3 and 4.

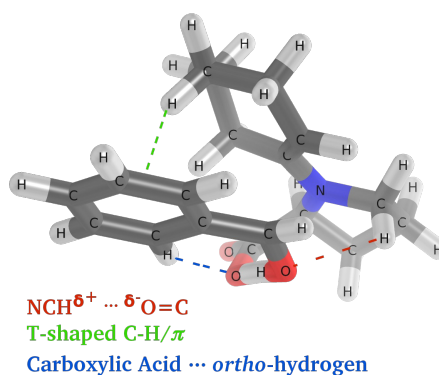


FIG. 4. The (*S,S*) *syn* 1 transition state, with the three hypothesized sources of non-covalent stabilization: $\text{NCH}^{\delta+} \cdots \delta^- \text{O}=\text{C}$, C-H/ π , and carboxylic acid \cdots *ortho*-hydrogen

Here we assess non-covalent stabilization in all 16 of Rzepa's transition state geometries for the proline-catalyzed aldol reaction. We directly compute the strength of interactions postulated^{3,4} to be important to transition state stabilization (see Figure 4) including (a) $\text{NCH}^{\delta+} \cdots \delta^- \text{O}=\text{C}$ electrostatic interactions between the NCH group of the pyrrolidinyllike fragment and the C=O bond of the aldehyde, (b) C-H/ π interactions between the cyclohexene ring of the enamine intermediate and the phenyl group of benzaldehyde, and (c) favorable electrostatic interactions between a $\delta^+ \text{H}$ *ortho*-hydrogen of the phenyl group from benzaldehyde and the hydroxyl oxygen of the carboxylic acid group of the enamine intermediate.

II. THEORETICAL METHODS

Symmetry-adapted perturbation theory (SAPT)⁷ offers the advantage of decomposing molecular interactions into components of electrostatics, exchange-repulsion, induction/polarization, and London dispersion forces. F-SAPT further improves upon this by providing interaction components for each pair of (user-defined) functional groups. Here we use F-SAPT based on the SAPT0 truncation of the perturbation series, which is essentially a second-order intermolecular perturbation theory based on a Hartree–Fock description of the monomers, in a developer’s version of PSI4.¹¹ Despite its lack of intramolecular correlation, SAPT0 provides reliable results for NCI¹² due to cancellation of errors when coupled with a jun-cc-pVDZ basis set,¹³ which is the standard Dunning aug-cc-pVDZ basis^{14,15} less diffuse functions on hydrogen atoms and d diffuse functions on heavy atoms.

For the present application to strongly interacting molecules (bonds are being formed and broken in the transition state), we have elected to use an exchange-scaled variant of SAPT0 denoted sSAPT0.¹² The exchange scaling is meant to correct for a breakdown of the perturbation theory for strongly interacting molecules.^{12,16,17} Exchange scaling was found to provide significantly better results for doubly hydrogen-bonded dimers.¹² The scaling affects the induction (via exchange-induction) and dispersion (via exchange-dispersion), although primarily the former. Electrostatics and pure exchange-repulsion terms are left unchanged.

Exchange-scaling is applied uniformly by replacing equation (30) from Ref. 18 by

$$S_{\delta} = \frac{E_{\text{ind,r}}^{(20)} + p_{\text{EX}}(3)E_{\text{exch-ind,r}}^{(20)}[S^2] + \delta_{\text{HF,r}}^{(2)}}{E_{\text{ind,r}}^{(20)} + E_{\text{exch-ind,r}}^{(20)}[S^2]}, \quad (1)$$

where

$$p_{\text{EX}}(\alpha) = \left(\frac{E_{\text{exch}}^{(10)}}{E_{\text{exch}}^{(10)}[S^2]} \right)^{\alpha}. \quad (2)$$

Similarly, all fragment exchange-dispersion energies are also scaled by $p_{\text{EX}}(3)$. This guarantees that the sum of the fragment contributions in F-SAPT recovers the same total induction and dispersion energies as computed in the parent sSAPT0 method.

The appropriate fitting basis sets were used for the density fitted algorithms: self-consistent field (SCF) procedure used jun-cc-pVDZ-JK, and two-body contributions from SAPT0 (dispersion and exchange-dispersion) used jun-cc-pVDZ-RI.¹⁹ Additionally, the core orbitals electrons of heavy atoms were constrained to be doubly occupied (“frozen”) in all computations.

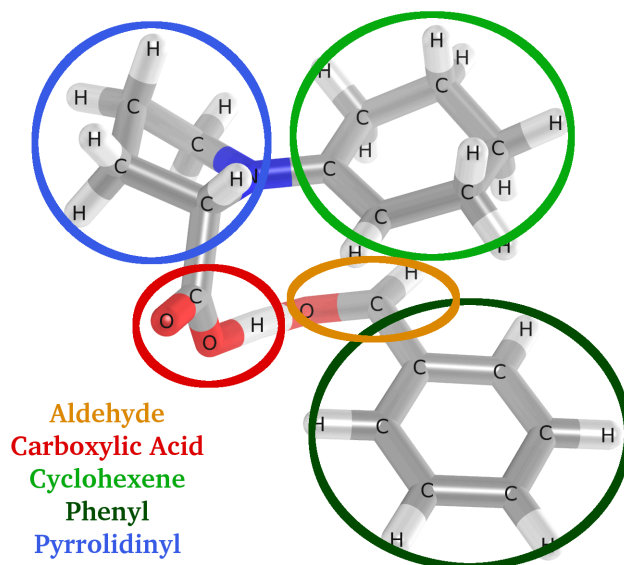


FIG. 5. The fragmentation scheme used for all F-SAPT analyses in this work, unless otherwise stated. There are five distinct fragments in total for the two monomers. Enamine intermediate: 1) carboxylic acid, 2) cyclohexene, 3) pyrrolidinyllike. Benzaldehyde: 4) aldehyde and 5) phenyl.

The transition state was partitioned into the functional groups shown in Figure 5 for F-SAPT analysis. As seen in Figures 2 and 5, a proton is being transferred from the carboxylic acid of the enamine intermediate to the benzaldehyde reactant. Standard SAPT (and F-SAPT) analysis requires two interacting monomers, and hence we partition the system into the original reactants for the purpose of the F-SAPT procedure. This choice avoids the positive and negative charges that would result from working with the monomers where the proton is accounted as already transferred, and these charges would tend to overwhelm other SAPT terms and thus complicate the analysis. For the F-SAPT analysis, benzaldehyde was considered as a phenyl group plus an aldehyde group, and the enamine intermediate was considered as a five membered pyrrolidinyllike nitrogen containing ring, a carboxylic acid group, and a cyclohexene ring. In this work, we use the transition state geometries previously obtained by Rzepa and co-workers.⁴

All molecular pictures generated using F-SAPT are colored with a red-white-blue color palette according to the interaction each functional group experiences with the included functional groups of the other monomer. Red signifies an attractive interaction, and blue

signifies a repulsive interaction. The color spectrum in all images becomes saturated at ± 25 kcal mol $^{-1}$ unless otherwise stated. Our F-SAPT analysis is supplemented in some cases by consideration of atomic charges, which we obtained using natural population analysis from NBO 5.0 in Q-Chem with the def2-TZVP basis set.²⁰⁻²²

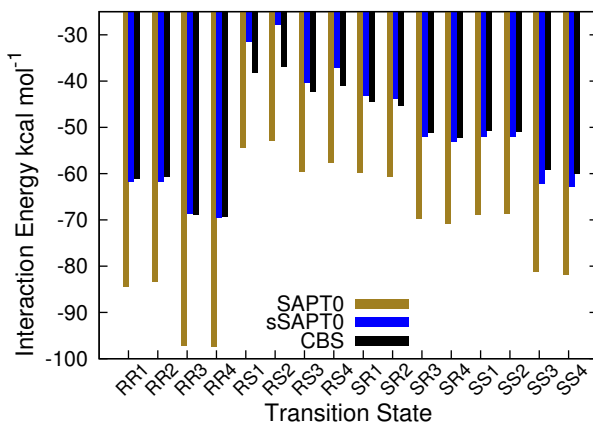


FIG. 6. Estimated CCSD(T)/CBS, SAPT0/jun-cc-pVDZ, and sSAPT0/jun-cc-pVDZ total interaction energies. CCSD(T)/CBS values were estimated as DF-MP2/aug-cc-pV(T,Q)Z + $\delta_{\text{MP2}}^{\text{CCSD(T)}}$ /cc-pVDZ.

This is the first application of F-SAPT to transition states, and so it is important to assess the reliability of the results, particularly because the intermolecular interaction will be strong in a transition state featuring bond breaking and/or bond forming between the SAPT monomers, as this one does. Figure 6 compares SAPT0/jun-cc-pVDZ and sSAPT0/jun-cc-pVDZ interaction energies of the two reacting molecules in the transition state to results from coupled-cluster theory with perturbative triple substitutions [CCSD(T)],²³ estimated in the complete-basis-set (CBS) limit using a focal-point approach.²⁴ Specifically, we estimate the CBS limit of second-order Møller-Plesset perturbation theory (MP2) and then correct this for higher-order correlation effects present in CCSD(T) but absent in MP2 by adding the difference between CCSD(T) and MP2, $\delta_{\text{MP2}}^{\text{CCSD(T)}}$, evaluated in a cc-pVDZ basis set. (Limited tests of evaluating $\delta_{\text{MP2}}^{\text{CCSD(T)}}$ in a larger aug-cc-pVDZ basis did not lead to significant differences). The MP2/CBS values were estimated using a standard two-point Helgaker extrapolation²⁵ of the correlation energies. MP2 and CCSD(T) results employed density-fitting approximations, and CCSD(T) results also employed MP2 frozen natural orbitals,²⁶ and truncated orbitals with occupation numbers less than 10^{-6} . All of these computations

were performed using PSI4.¹¹

The comparison in Figure 6 shows that both SAPT0 and sSAPT0 provide similar *trends* as high-level CCSD(T)/CBS for the interaction energies. Indeed, both SAPT0 and sSAPT0 give nearly the same energetic ordering of the transition states, with some rearrangements among transition states with nearly identical interaction energies (this is also illustrated in a plot of the relative interaction energies, Figure S1 of the Supplementary Information). However, the SAPT0 interaction energies are substantially too strong (by tens of kcal mol⁻¹). As discussed above, one would expect difficulties for SAPT when the monomers are strongly interacting, as they are here for reacting molecules. However, exchange-scaled sSAPT0, which has been shown to improve interaction energy estimates for doubly hydrogen-bonded systems,¹² is seen to drastically improve the SAPT results relative to CCSD(T)/CBS. With the exception of (*R,S*) *ent-anti* 1 and (*R,S*) *ent-anti* 2 being substantially less bound (~ 7 -9 kcal mol⁻¹), the other transition states feature an excellent agreement between sSAPT0/jun-cc-pVDZ and CCSD(T)/CBS (within 1-4 kcal mol⁻¹ out of interaction energies of 37-69 kcal mol⁻¹).

We expect the largest errors in the F-SAPT analysis to be for the aldehyde \cdots carboxylic acid pair, where a proton is being transferred, and for the aldehyde \cdots cyclohexene pair, where a C-C bond is being formed. Fortunately, the three hypothesized sources of NCI stabilization in the literature that are the focus of the present study are not between those pairs of functional groups.

III. RESULTS AND DISCUSSION

Rzepa and co-workers recognized⁴ three sources of non-covalent stabilization using a density-based analysis.⁶ As illustrated in Figure 4, they were as follows:

1. Significant stabilization between the oxygen of the aldehyde and a nearby hydrogen on the pyrrolidinyll fragment in (*S,R*) *anti* and (*S,S*) *syn* transition states [NCH ^{$\delta+$} \cdots δ^- O=C]. Houk and co-workers noticed these close contacts in their original study³ and argued that they were key in the selectivity to the (*S,R*) *anti* and (*S,S*) *syn* transition states. The authors attribute this to be the dominant NCI contact of the aforementioned transition states due to its electrostatic nature.

2. A CH/ π hydrogen bond interaction between a hydrogen on cyclohexene and the phenyl group on benzaldehyde for the (S,S) *syn* transition states.
3. The (S,S) *syn* transition states exhibit a stabilizing interaction between the *ortho*-hydrogen on the phenyl group of benzaldehyde with the hydroxyl oxygen of carboxylic acid.

Below we directly assess each of these reported sources of NCI transition state stabilization using F-SAPT.

A. $\text{NCH}^{\delta+} \dots \delta^- \text{O}=\text{C}$ Interactions

A geometric inspection of the transition states shows that (S,S) and (S,R) are likely to exhibit the strongest interaction between the NCH on the pyrrolidinyll fragment and the C=O on the aldehyde. This is due to the hydrogen in NCH being within 2.43 - 2.59 Å of the aldehyde oxygen for both transition states. (R,R) and (R,S) both have longer contact distances, from 3.10 - 3.22 Å, which likely leads to a weaker interaction in these transition states.

Electrostatics:

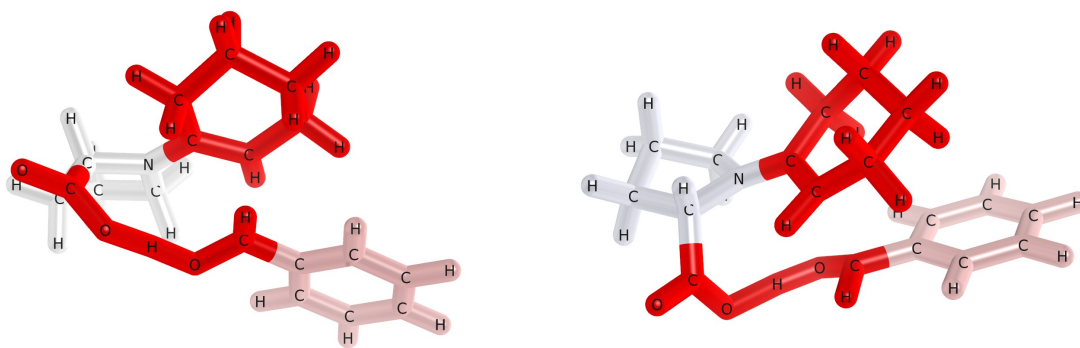


FIG. 7. The electrostatic interaction between the benzaldehyde monomer and the entire enamine intermediate is visualized for (S,R) *anti* 1 (left) and (R,R) *ent-syn* 1 (right) using the terms from an F-sSAPT0/jun-cc-pVDZ decomposition. Deeper red indicates a stronger attraction, and deeper blue indicates stronger repulsion.

Figure 7 provides a visual representation of the electrostatic interactions between the reacting molecules in two of the transition states considered, namely the (*S,R*) 1 and (*R,R*) 1 conformers. Figure S3 in the Supplementary Information displays the results for all 16 transition states. As previously mentioned, these F-SAPT figures are color coded such that red fragments are attracted to the other monomer, and blue fragments are repulsed by the other monomer; white fragments have net interaction energies near zero. Surprisingly, the hypothesized electrostatic stabilization between the $\text{NCH}^{\delta+}$ group of the pyrrolidinyl fragment and the $\delta^- \text{O}=\text{C}$ carbonyl group of the aldehyde is not evident in the F-SAPT visualizations. Instead, the pyrrolidinyl fragment is nearly white for the two conformers of Figure 7, and remains nearly white or slightly blue for all the other conformers in Figure S3; this indicates that the pyrrolidinyl fragment has no net electrostatic attraction to the benzaldehyde. The aldehyde group is deep red for all 16 transition states, indicating a strong attraction to the enamine intermediate; however, from the color coding of the enamine intermediate, evidently the stabilizing interactions with the aldehyde group involve primarily the transferring proton from the carboxylic acid and the bond formation with the cyclohexene ring.

Figure 8 presents a breakdown of the interactions between each fragment in benzaldehyde (the aldehyde and phenyl groups) with each fragment of the enamine intermediate (the pyrrolidinyl group, the carboxylic acid group, and the cyclohexene ring). The Aldehyde ... Pyrrolidinyl panel of Figure 8 displays the interaction energy components between the aldehyde group and the pyrrolidinyl group, and it confirms that the electrostatic interaction is repulsive (in the range of 0-2 kcal mol⁻¹) for all transition states considered.

Houk and List³ expected the (*S,R*) and (*S,S*) transition states to be more stabilized by $\text{NCH}^{\delta+} \cdots \delta^- \text{O}=\text{C}$ interactions than (*R,R*) and (*R,S*) transition states due to their closer H ... O contacts. According to Figure 8, the (*S,R*) and (*S,S*) geometries exhibit somewhat less repulsive electrostatics in general, but there are several exceptions for particular conformers.

Given the disagreement between the F-SAPT results and the expectations from the literature regarding the favorability of the $\text{NCH}^{\delta+} \cdots \delta^- \text{O}=\text{C}$ contacts, we examined these interactions in more detail by computing atomic charges for the transition state geometries using a natural population analysis (NPA) at the B3LYP/def2-TZVP level of theory. Atom-centered point charges are a rather crude representation of the true electrostatic interactions, but such an analysis is easier to understand. Figure 9 presents the atomic charges for the most relevant atoms to the $\text{NCH}^{\delta+} \cdots \delta^- \text{O}=\text{C}$ contact for the (*S,R*) 1 transition state; re-

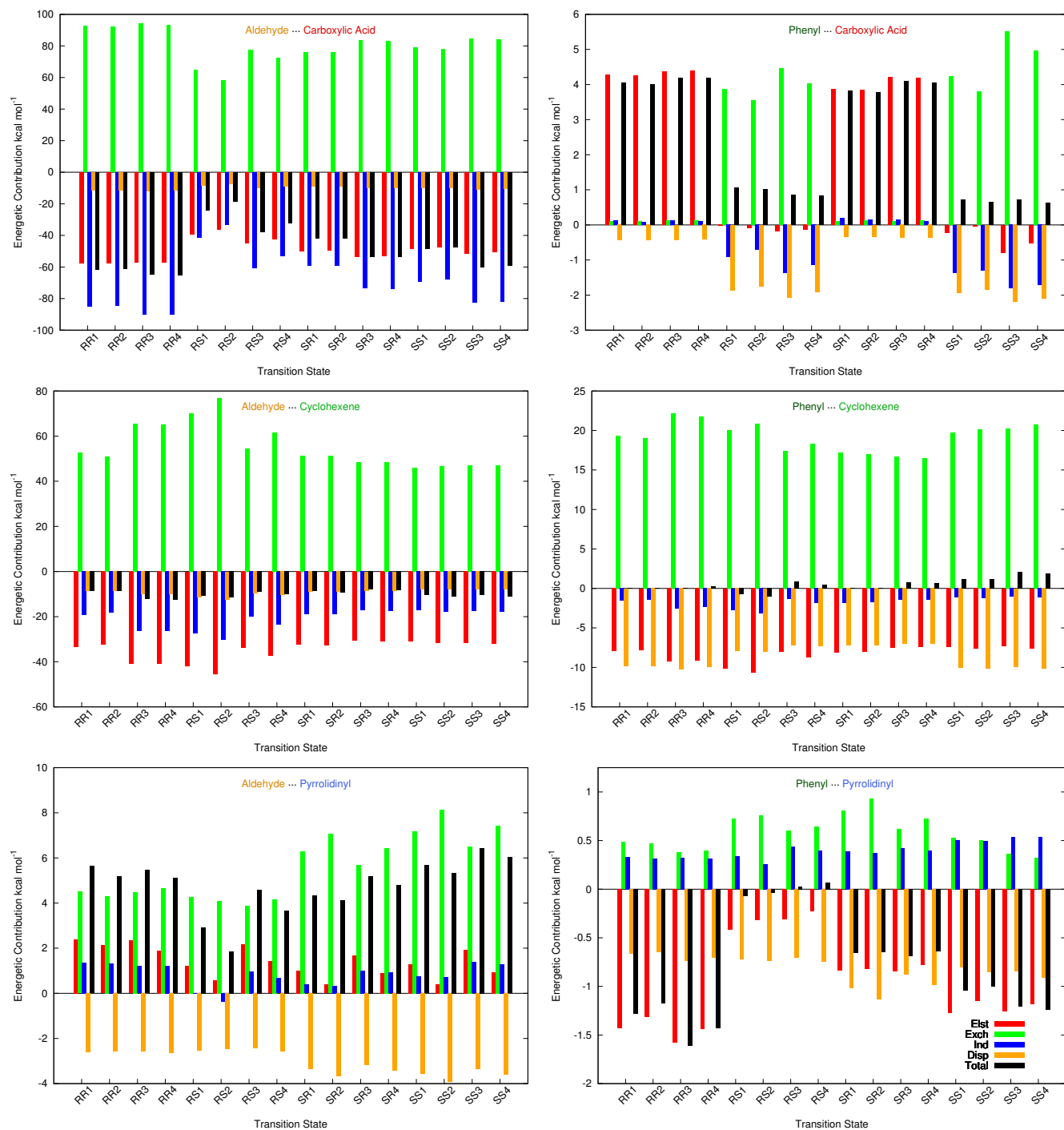


FIG. 8. The F-SAPT predicted energetic components of the interaction between each of the fragments are plotted at the sSAPT0/jun-cc-pVDZ level of theory.

results for the other transition states are similar, and a summary of the Coulomb interactions for all transition states is presented in Figures S8-S11 of the Supplementary Information.

Using the NPA charges, the Coulomb interaction between the nearest hydrogen of the

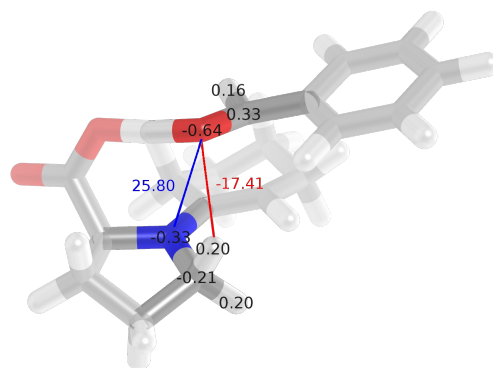


FIG. 9. The primary charges involved in determining the favorability of the interaction between $\text{NCH}^{\delta+}$ of the enamine intermediate and $\delta^- \text{O}=\text{C}$ of benzaldehyde for the (*S,R*) *anti* 1 transition state.

NCH_2 group and the oxygen of the aldehyde group is, as expected, strongly attractive (~ 17 - 19 kcal mol^{-1} for the geometries with a close contact, and ~ 14 - 16 kcal mol^{-1} for geometries with a farther contact). However, the interaction between the pyrrolidinyl nitrogen and the aldehyde oxygen is repulsive and of even greater magnitude (~ 24 - 26 kcal mol^{-1}). In the point-charge model, next most attractive contacts are (1) the more distant hydrogen of the NCH_2 interacting with the aldehyde oxygen (~ 9 - 12 kcal mol^{-1}), and (2) the negatively charged carbon of NCH_2 interacting with the positively charged aldehyde carbon (~ 5 - 7 kcal mol^{-1}). These favorable contacts are canceled out by the interaction of the aldehyde oxygen with the negative NCH_2 carbon (~ 13 - 15 kcal mol^{-1}) and by the repulsion between the positive aldehyde carbon and the positive NCH_2 hydrogens (~ 4 to 8 kcal mol^{-1} per contact). Other attractive interactions ($\text{N} \cdots \text{H}$, $\text{C} \cdots \text{H}$, $\text{C} \cdots \text{C}$) are much weaker and are not sufficient to overcome the strength of the repulsive interactions.

Thus the F-SAPT analysis does not confirm the hypothesized electrostatic stabilization due to $\text{NCH}^{\delta+} \cdots \delta^- \text{O}=\text{C}$ contacts. Instead, the electrostatic interaction between the aldehyde group and the pyrrolidinyl group is found to be slightly repulsive. (This remains true if we perform alternative F-SAPT computations in which we isolate just the NCH_2 group of the pyrrolidinyl ring, instead of treating the pyrrolidinyl group as a whole). A simple

analysis using atom-centered charges shows that although the $\text{H}^{\delta+} \cdots \text{O}^{\delta-}$ interaction is attractive as expected, the nitrogen is sufficiently negative that the $\text{N}^{\delta-} \cdots \text{O}^{\delta-}$ overcomes this attraction, and the overall electrostatics are repulsive.

Having analyzed the electrostatics of the aldehyde \cdots pyrrolidinyl interaction in detail, let us consider the other fundamental components of the interaction. In Figure 8 we see that the most attractive interaction between these groups is not electrostatics, but London dispersion forces ($\sim 2\text{-}4 \text{ kcal mol}^{-1}$). Dispersion is somewhat more favorable for the (S,R) and (S,S) transition states than for the other stereoisomers. This is presumably a result of the closer $\text{NCH} \cdots \text{O}=\text{C}$ contacts in these geometries. On the other hand, these geometries also feature larger exchange-repulsion, so that the overall aldehyde \cdots pyrrolidinyl interaction is not more favorable for these transition states. Induction is weakly destabilizing or near zero for most of the transition states. (The overall induction term must be attractive instead of repulsive, but when we look at any pair of fragments in F-SAPT, the contribution from that particular pair can be repulsive; this just means that the polarization of each monomer in response to the other monomer leads to a new electron distribution that is overall more favorable, but from the point of view of certain functional groups, the local interaction might become less favorable).

The total aldehyde \cdots pyrrolidinyl interaction energies are overall repulsive, and roughly similar across all transition states except for (R,S) 1 and (R,S) 2, which are noticeably less destabilized than the others. These two conformers feature among the least destabilizing exchange-repulsion and electrostatic terms, perhaps because they are among those with the *longer* $\text{NCH} \cdots \text{O}=\text{C}$ contacts. The relative favorability of these two conformers for the aldehyde \cdots pyrrolidinyl part of the NCI between the reactants does not correlate with the experimentally observed preference for the (S,R) and (S,S) products.

B. C–H/ π Interaction

Attractive C–H/ π interactions between an aliphatic C–H group and an aromatic π system have been observed in many systems,²⁷ and Krenske and Houk have argued that they may control the stereochemical outcome of numerous addition reactions involving aromatic substituents.²⁸ These interactions are typically stabilizing by ~ 1 to 5 kcal mol^{-1} , and previous work using SAPT suggests²⁹ that this stabilization arises from two sources: (1) London

Dispersion:

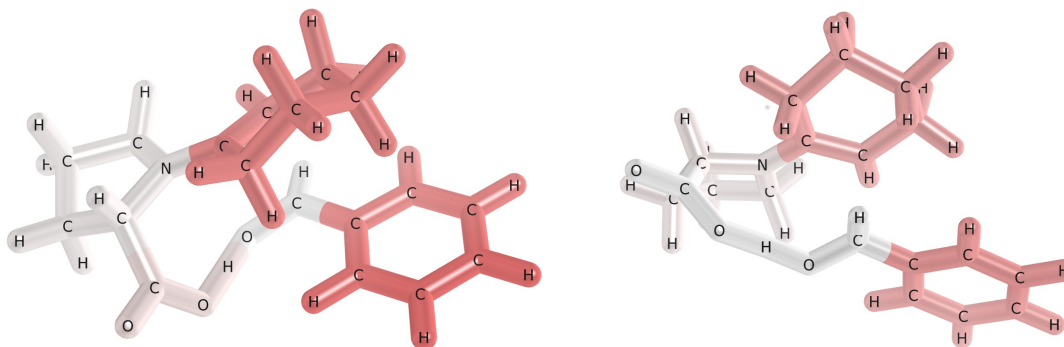


FIG. 10. The dispersion interaction between the phenyl group and the entire enamine intermediate is visualized for (*S,S*) *syn* 1 (left) and (*S,R*) *anti* 1 (right) using our F-sSAPT0/jun-cc-pVDZ decomposition. In this figure, aldehyde interactions are excluded.

dispersion forces, and (2) an electrostatic attraction between the partial positive charge on the hydrogen and the negatively charged π face of the aromatic. Dispersion contributions are about 1.6x larger than electrostatic contributions for the prototype $\text{CH}_4 \cdots \text{benzene}$ interaction.²⁹

Rzepa and co-workers⁴ claim that C–H/ π interactions lead to large dispersion stabilization for the (*S,S*) transition states. Indeed, geometric analysis of these transition states shows a favorable C–H/ π contact geometry; the nearest C–H bond is directly over and oriented towards the π cloud of the phenyl group, and with contact distances of 2.58 - 2.65 Å between the nearest hydrogen of cyclohexene and the center of mass of the carbons of the phenyl ring. This favorable contact could help explain the experimental preference for (*S,S*) products, although not the nearly equal amount of (*S,R*) products. However, geometric analysis also shows similarly favorable C–H/ π interactions (2.58 - 2.72 Å separation) for the (*R,R*) transition states, which do not lead to an experimentally favored product. For the other transition state stereoisomers, the C–H/ π arrangement is not as favorable, and the contact distances are typically larger, 3.21 - 3.38 Å.

The presence of favorable C–H/ π contacts between the phenyl and cyclohexene groups is also supported by the dispersion and electrostatic components of our F-SAPT analysis.

Figure 10 illustrates a stronger dispersion interaction between cyclohexene and the phenyl group for the (S,S) 1 geometry, which features a close C–H/ π contact, than in the (S,R) 1 transition state, which does not. (For simplicity, this figure shows the F-SAPT dispersion only between the phenyl group and the enamine intermediate, with the aldehyde contributions suppressed.)

The Phenyl \cdots Cyclohexene panel of Figure 8 displays each component of the phenyl \cdots cyclohexene interaction for all 16 transition states, and it confirms that the geometries with the closer C–H/ π contacts, (S,S) and (R,R) , have greater dispersive stabilization (~ 10 kcal mol $^{-1}$) than the (R,S) and (S,R) geometries ($\sim 7-8$ kcal mol $^{-1}$). All transition states have similar, stabilizing electrostatic contributions ($\sim 7-8$ kcal mol $^{-1}$) except for (R,R) 3, (R,R) 4, (R,S) 1, and (R,S) 2 ($\sim 9-10$ kcal mol $^{-1}$). In all cases where a favorable C–H/ π interaction is expected, the dispersion contribution is 1.1 to 1.4 times greater than electrostatics, roughly in accordance with the 1.6 ratio for CH $_4$ \cdots benzene.²⁹ Induction contributions are stabilizing or close to zero for all transition states.

Thus, for the attractive components of the interaction, there seems to be a preference for the (S,S) and (R,R) transition state stereoisomers, consistent with their more favorable C–H/ π geometries, although the (R,S) 1 and (R,S) 2 conformers are also rather favorable due to their having the most attractive electrostatic interactions. Unfortunately, however, the transition states with the most favorable attractive components are not necessarily the ones with the most favorable *total* interaction energies. For the phenyl \cdots cyclohexene interactions, Figure 8 shows that the transition states with the most favorable attractions also tend to have the most unfavorable exchange-repulsion terms, so that the net interaction energies are all small. The (R,S) 1 and (R,S) 2 transition states are most stabilized (~ 1 kcal mol $^{-1}$) while (S,S) 3 and (S,S) 4 are the most destabilized (~ 2 kcal mol $^{-1}$). All other transition states are either negligibly stabilized or destabilized by about 1 kcal mol $^{-1}$ or less. Unfortunately, and perhaps surprisingly, these results for the total interaction energies between the phenyl and cyclohexene groups do not correlate with the presence or absence of good C–H/ π contacts.

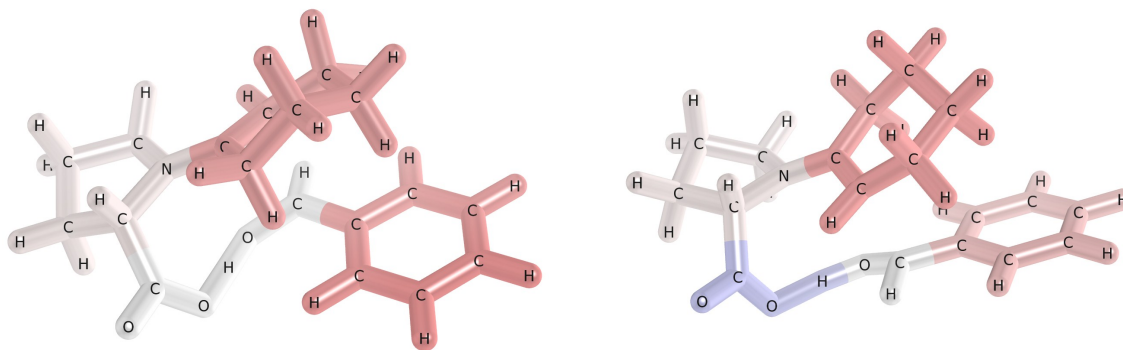
Electrostatics:

FIG. 11. The electrostatic interaction between the phenyl group and the enamine intermediate is visualized for (S,S) *syn* 1 (left) and (R,R) *ent-syn* 1 (right) at the F-sSAPT0/jun-cc-pVDZ level of theory. In this figure, aldehyde interactions are excluded.

C. Phenyl *ortho*-Hydrogen \cdots Carboxylic Acid

A geometric inspection of the transition states for the *ortho*-hydrogen \cdots carboxylic acid contact reveals contact distances of 2.18-2.32 Å for (S,S) and (R,S) transition states. In these transition states, the *ortho*-hydrogen is oriented towards an oxygen in the carboxylic acid, while the (S,R) and (R,R) transition states feature an *ortho*-hydrogen that is neither close (~ 4.9 Å) nor oriented correctly. Therefore, we expect to see non-covalent stabilization through electrostatics and dispersion for (S,S) and (R,S) transition states but not (S,R) and (R,R) .

An F-SAPT illustration of this interaction is presented in Figure 11; aldehyde interactions have been suppressed for simplicity. The (S,S) transition state pictured has a red phenyl group, indicating that it interacts favorably with the enamine intermediate. A significant part of this favorable electrostatic interaction is actually due to the cyclohexenyl group, as indicated by its red color. The carboxylic acid group is nearly white, indicating little net electrostatic attraction between it and the phenyl group. However, in the (R,R) transition state pictured in the right of Figure 11, the phenyl group is less red (less favorable interactions with the enamine intermediate) and the carboxylic acid group is now slightly blue, indicating an unfavorable electrostatic interaction with the phenyl group. Hence, the close contact and

favorable alignment between the phenyl *ortho*-hydrogen and the carboxylic oxygen allows for a favorable electrostatic contact that compensates for an otherwise unfavorable phenyl \cdots carboxylic interaction.

More detail is provided by Figure 8, which presents all the components for the phenyl \cdots carboxylic interaction for all 16 transition state conformers. The Figure shows a dramatic difference between the (R,S) and (S,S) transition states vs. the (S,R) and (R,R) transition states. The (R,S) and (S,S) geometries experience significant dispersion stabilization (~ 2 kcal mol $^{-1}$), whereas this stabilization is about 0.5 kcal mol $^{-1}$ or less for other geometries. Likewise, (R,S) and (S,S) geometries feature significant stabilizing induction contributions (1-2 kcal mol $^{-1}$), whereas induction is negligible for other geometries. The electrostatic contributions for (S,R) and (R,R) geometries are destabilizing by about 4 kcal mol $^{-1}$, whereas they are about zero or weakly stabilizing for (R,S) and (S,S) geometries. The significantly more favorable attractive interactions between the phenyl and carboxylic acid groups in the (R,S) and (S,S) transition states are opposed by larger exchange-repulsion contributions, which are typically around 4-5 kcal mol $^{-1}$; exchange-repulsion is nearly negligible for the (S,R) and (R,R) geometries. Nevertheless, the overall interaction energies between the phenyl and carboxylic acid groups are substantially less repulsive for the (R,S) and (S,S) transition states, which feature close contacts between the phenyl *ortho*-hydrogen and the hydroxyl oxygen of the carboxylic acid.

D. Summary of Non-Covalent Interactions

A seemingly favorable $\text{NCH}^{\delta+} \cdots \delta^{-}\text{O}=\text{C}$ interaction, identified by geometric analysis³ and apparently confirmed by electron-density-based analysis⁴ using the NCIPLOT program,⁵ exists in the (S,R) and (S,S) transition states, which correspond to the experimentally favored stereoisomer products. However, in this case apparently the correlation is fortuitous, because direct computation of the interaction between the aldehyde and pyrrolidinyl fragments yields repulsive interaction energies, with similar values for all transition states except for smaller destabilization for the (R,S) 1 and (R,S) 2 conformers. The expected electrostatic attraction between the $\text{NCH}^{\delta+}$ and $\delta^{-}\text{O}=\text{C}$ moieties is found to actually be repulsive due to the large partial negative charge on the nitrogen.

An aromatic CH/π interaction between a hydrogen on the cyclohexene ring and the phenyl

group of benzaldehyde was noted⁴ for the (*S,S*) transition states, which correspond to one of the two favored products. However, this contact also exists for the unfavored (*R,R*) transition states. The dispersion component of the F-SAPT analysis shows a preference for these stereoisomers, while the electrostatic interaction is similar for all stereoisomers except for a preference for two (*R,R*) and two (*R,S*) conformers. However, when all SAPT components are added up, the overall interaction energies between the cyclohexene and phenyl groups are actually more favorable for the (*R,S*) 1 and (*R,S*) 2 conformers, which lack the proposed CH/ π interaction.

Finally, density-based analysis with NCIPLLOT also suggested favorable stabilizing interactions between an *ortho*-hydrogen of the phenyl ring and the hydroxyl oxygen of the carboxylic acid.⁴ This interaction is present in the (*S,S*) and (*R,S*) transition states. F-SAPT analysis clearly supports the favorability of these contacts, which lead to substantially more favorable non-covalent interactions between the phenyl and carboxylic acid groups in these stereoisomers.

Thus, out of three hypothesized stabilizing interactions, one turns out to be destabilizing, another turns out to be canceled by exchange-repulsion forces, and only the third is confirmed by direct computation. The overall interaction between the pyrrolidinyl and aldehyde groups favors the (*R,S*) 1 and (*R,S*) 2 conformers, as does the overall interaction between the cyclohexene and phenyl groups. Unfortunately, these are not the experimentally favored stereoisomers of the products. The overall interaction between the phenyl and carboxylic acid groups favors the (*S,S*) and (*R,S*) stereoisomers. While the (*S,S*) stereoisomers are one of the favored products experimentally, the (*R,S*) isomers are not. Thus, none of the hypothesized non-covalent interactions seems to control the stereoselectivity.

Figure 12 presents the total SAPT interaction energies between the two reacting molecules, summed over all interacting pairs of fragments. The total SAPT interaction energies are similar for many of the transition states, but with a noticeable preference for the (*R,R*) stereoisomers and a less pronounced preference for the (*S,S*) 3 and (*S,S*) 4 conformers. The stronger stabilizing interaction energies for the (*R,R*) stereoisomers are primarily a result of a preference for these stereoisomers in the very strong interaction between the reacting aldehyde and carboxylic acid groups (see Fig. 8). We note that the *total* SAPT interaction energies also fail to correlate well with the experimentally observed preference for (*S,R*) and (*S,S*) products. This strongly suggests that stereoselectivity in this reaction is not solely

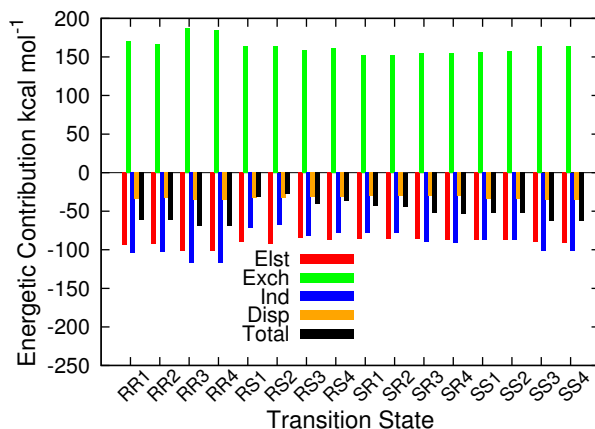


FIG. 12. The total SAPT decomposition of the energetics in each transition state is plotted at the sSAPT0/jun-cc-pVDZ level of theory. This plot only accounts for total monomer interactions, meaning the energetics are for the whole enamine intermediate interacting with benzaldehyde.

governed by non-covalent interactions, but is also substantially influenced by deformation energies (the other half of the “distortion-interaction” model of transition states¹ mentioned in the introduction).

E. Distortion Analysis

Table II presents the CCSD(T)/CBS deformation energies and (counterpoise-corrected) interaction energies for the 16 transition state conformers. The distortion energies are very significant and range from 43–80 kcal mol⁻¹. The largest distortion in the transition state appears to be the breaking of the carboxylic acid O–H bond, as the proton is transferred to the carbonyl of benzaldehyde. In the enamine intermediate, this bond length is $R_e = 0.98$ Å, whereas in the transition state it varies from 1.14 to 1.39 Å. We found a good correlation ($R^2=0.92$) between the deformation energy and $(R - R_e)^2$ for this bond (see Figure S2 of the Supplementary Information). From our analysis, other key geometrical characteristics (C=O bond length of benzaldehyde, N-C bond length of proline intermediate, bond angle of C-O-H on carboxylic acid) seem to be relatively constant for each transition state, and do not correlate well with the change in deformation energy.

F. Comparison to Experiment

Our primary goal in this paper has been to directly analyze the proposed non-covalent interactions in the Houk-List model of proline-catalyzed aldol reactions. However, given that we have computed CCSD(T)/CBS energies for the transition states, it is interesting to explore whether these higher-level results exhibit better agreement with experimental product ratios than the B3LYP-D3/TZVP/SCRF=DMSO results of Rzepa and co-workers.⁴ That study predicted a product ratio of 99.3 (*S,R*) : 0.7 (*S,S*), compared to an experimental³ ratio of 45-47 : 43-45. However, before going further, it is important to point out a caution raised by Rzepa and co-workers: “repetition of the experimental results by List found product selectivities to vary, with the reaction found to be extremely sensitive to both water content and to temperature.”⁴ Hence, it is probably not realistic to expect close agreement between theory and experiment.

Table I presents the relative electronic energies of the transition states computed at the B3LYP-D3/TZVP/SCRF=DMSO level of theory (ΔE_{solv}) and the corresponding relative Gibbs free energies at 298K ($\Delta\Delta G_{\text{solv}}$). We then present results using our gas-phase CCSD(T)/CBS estimates for the transition state energies (ΔE_{gas}). It is difficult to perform solvent corrections and/or thermodynamic corrections to our bare electronic energy differences at the coupled-cluster level due to computational expense, so we simply applied these corrections as determined by Rzepa and co-workers at the B3LYP-D3/TZVP/SCRF=DMSO level to obtain approximate CCSD(T)/CBS $\Delta\Delta G_{\text{solv}}$ values.

The $\Delta\Delta G_{\text{solv}}$ values are fairly consistent between the B3LYP-D3/TZVP and CCSD(T)/CBS levels of theory, although differences can be as large as 2.2 kcal mol⁻¹. Nevertheless, predicted product ratios are very similar between B3LYP-D3/TZVP and CCSD(T)/CBS; both predict about 99% of (*S,R*) and about 1% of (*S,S*). Unfortunately this leaves the discrepancy with experiment unresolved (although one must keep in mind the uncertainty in the experimental values). We note that Rzepa and co-workers did not seek any pre-reactive complexes of the two reactants; if such complexes experience significant stabilization, they might influence the relative barrier heights and hence the product ratios. Additionally, the noticeable differences in energetics between the B3LYP-D3/TZVP and CCSD(T)/CBS might be taken to indicate that the B3LYP-D3/TZVP transition state geometries might change significantly if they could be re-optimized at higher levels of theory (unfortunately,

this would be rather expensive computationally).

IV. CONCLUSIONS

The “distortion-interaction” model¹ and the “activation strain” model² state that transition state energetics are determined by non-covalent interaction energies and by the energy required to deform the reactants into the transition state geometry. In principle, a better understanding of non-covalent interactions could be used to reduce barrier heights and/or control stereoselectivity. The recently-developed functional-group partitioning of symmetry-adapted perturbation theory (F-SAPT)¹⁰ provides a theoretical tool for directly computing non-covalent interactions between pairs of functional groups. The present study represents its first application to analyzing non-covalent interactions in transition states. We have studied the proline-catalyzed aldol reaction between benzaldehyde and cyclohexanone as a simple model system for which several stabilizing non-covalent interactions have been hypothesized to play a role in stereoselectivity.

Of the three previously-hypothesized stabilizing non-covalent interactions, F-SAPT confirms only one, a favorable contact between an *ortho*-hydrogen of the phenyl group and the hydroxyl oxygen of the carboxylic acid. A hypothesized CH/ π interaction between a hydrogen of cyclohexene and phenyl is found to have favorable attractive terms but is canceled by unfavorable exchange-repulsion terms. A hypothesized stabilizing NCH ^{δ^+} ... ^{δ^-} O=C contact thought to control stereoselectivity is found to actually be repulsive due to the negative charge on the nitrogen. These contacts were thought to be stabilizing on the basis of a geometric analysis of the transition state and chemical intuition, and/or on the basis of electron density analysis via the NCIPLOT program,⁵ which relies on correlations between the properties of the electron density and what are typically found to be favorable non-covalent interactions. The reaction studied appears to provide a challenge for such geometry and/or density-based analysis.

The SAPT0 method that underlies our F-SAPT approach is also challenged by the transition states studied; its usual accuracy when paired with the jun-cc-pVDZ basis¹² is degraded substantially for the present system, no doubt because the transferring proton and the forming carbon-carbon bond lead to a very strong interaction between the monomers (the theory assumes modest to weak interactions). SAPT0 provides essentially the same

relative ordering as high-level CCSD(T)/CBS, so that it may remain suitable for analyzing trends. However, we can nearly eliminate the errors in the interaction energies using the exchange-scaled sSAPT0 method, which has previously been shown to improve over SAPT0 for strongly-interacting doubly hydrogen-bonded dimers.¹² sSAPT0/jun-cc-pVDZ provides excellent agreement with CCSD(T)/CBS for both the ordering and the values of the transition state interaction energies. Hence, for this study we modified the F-SAPT approach to partition sSAPT0 interaction energies.

Whether one uses SAPT or the high-quality CCSD(T)/CBS results, *interaction energies* between the two reactants do not correlate well with either the experimentally observed product ratios or with the differences between the CCSD(T)/CBS *total energies* of the transition states, which include geometry deformation effects. This indicates that, for the present reaction, the “distortion” terms of the “distortion-interaction” model are at least as important as the interaction terms for understanding stereoselectivity. Indeed, the distortion terms range from 43-80 kcal mol⁻¹ at the CCSD(T)/CBS level of theory, and they strongly correlate with $(R - R_e)^2$ for the breaking O-H bond of the carboxylic acid group. It remains to be seen whether other classes of reactions are more completely controlled by the non-covalent interaction terms.

Relative energies of the transition states computed with CCSD(T)/CBS are in reasonably good agreement with previous B3LYP-D3/TZVP results. Either approach, when corrected for solvent effects and thermodynamic corrections, estimates around a 99:1 product ratio for $(S,R) : (S,S)$ stereoisomers, compared to experimental results showing a roughly equal proportion of these isomers. The experiments are known to be very sensitive to the reaction conditions, which may partially explain this disagreement. In addition, improved theoretical values may be obtained by searching for pre-reactive complexes and/or obtaining higher-quality transition state geometries.

ACKNOWLEDGMENTS

This work was supported by the US Department of Energy, Office of Basic Energy Science, through catalysis contract No. DE-FG02-03ER15459.

REFERENCES

- ¹D. H. Ess and K. N. Houk, *J. Am. Chem. Soc.*, 2007, **129**, 10646–10647.
- ²I. Fernández and F. M. Bickelhaupt, *Chem. Soc. Rev.*, 2014, **43**, 4953–4967.
- ³S. Bahmanyar, K. N. Houk, H. J. Martin and B. List, *J. Am. Chem. Soc.*, 2003, **125**, 2475–2479.
- ⁴A. Armstrong, R. A. Boto, P. Dingwall, J. Contreras-Garcia, M. J. Harvey, N. J. Mason and H. S. Rzepa, *Chem. Sci.*, 2014, **5**, 2057–2071.
- ⁵J. Contreras-García, E. R. Johnson, S. Keinan, R. Chaudret, J. Piquemal, D. N. Beratan and W. Yang, *J. Chem. Theory Comput.*, 2011, **7**, 625–632.
- ⁶E. R. Johnson, S. Keinan, P. Mori-Sanchez, J. Contreras-Garcia, A. J. Cohen and W. Yang, *J. Am. Chem. Soc.*, 2010, **132**, 6498–6506.
- ⁷B. Jeziorski, R. Moszynski and K. Szalewicz, *Chem. Rev.*, 1994, **94**, 1887–1930.
- ⁸K. Szalewicz, *WIREs Comput. Mol. Sci.*, 2012, **2**, 254–272.
- ⁹C. D. Sherrill, *Acc. Chem. Res.*, 2013, **46**, 1020–1028.
- ¹⁰R. M. Parrish, T. M. Parker and C. D. Sherrill, *J. Chem. Theory Comput.*, 2014, **10**, 4417–4431.
- ¹¹J. M. Turney, A. C. Simmonett, R. M. Parrish, E. G. Hohenstein, F. A. Evangelista, J. T. Fermann, B. J. Mintz, L. A. Burns, J. J. Wilke, M. L. Abrams, N. J. Russ, M. L. Leininger, C. L. Janssen, E. T. Seidl, W. D. Allen, H. F. Schaefer, R. A. King, E. F. Valeev, C. D. Sherrill and T. D. Crawford, *WIREs Comput. Mol. Sci.*, 2012, **2**, 556–565.
- ¹²T. M. Parker, L. A. Burns, R. M. Parrish, A. G. Ryno and C. D. Sherrill, *J. Chem. Phys.*, 2014, **140**, 094106.
- ¹³E. Papajak, J. Zheng, X. Xu, H. R. Leverentz and D. G. Truhlar, *J. Chem. Theory Comput.*, 2011, **7**, 3027–3034.
- ¹⁴T. H. Dunning, *J. Chem. Phys.*, 1989, **90**, 1007–1023.
- ¹⁵R. A. Kendall, T. H. Dunning and R. J. Harrison, *J. Chem. Phys.*, 1992, **96**, 6796–6806.
- ¹⁶K. U. Lao and J. M. Herbert, *J. Phys. Chem. A*, 2012, **116**, 3042–3047.
- ¹⁷R. Schaeffer and G. Jansen, *Mol. Phys.*, 2013, **111**, 2570–2584.
- ¹⁸R. M. Parrish and C. D. Sherrill, *J. Chem. Phys.*, 2014, **141**, 044115.
- ¹⁹F. Weigend, M. Kattannek and R. Ahlrichs, *J. Chem. Phys.*, 2009, **130**, 164106.
- ²⁰F. Weigend, *Phys. Chem. Chem. Phys.*, 2006, **8**, 1057–1065.

- ²¹E. D. Glendening, J. K. Badenhop, A. E. Reed, J. E. Carpenter, J. A. Bohmann, C. M. Morales and F. Weinhold, *NBO 5.0*, Theoretical Chemistry Institute: University of Wisconsin, Madison, WI, 2001, <http://www.chem.wisc.edu/~nbo5>.
- ²²Y. Shao, Z. Gan, E. Epifanovsky, A. T. B. Gilbert, M. Wormit, J. Kussmann, A. W. Lange, A. Behn, J. Deng, X. Feng, D. Ghosh, M. Goldey, P. R. Horn, L. D. Jacobson, I. Kaliman, R. Z. Khaliullin, T. Kus, A. Landau, J. Liu, E. I. Proynov, Y. M. Rhee, R. M. Richard, M. A. Rohrdanz, R. P. Steele, E. J. Sundstrom, H. L. Woodcock, P. M. Zimmerman, D. Zuev, B. Albrecht, E. Alguire, B. Austin, G. J. O. Beran, Y. A. Bernard, E. Berquist, K. Brandhorst, K. B. Bravaya, S. T. Brown, D. Casanova, C. Chang, Y. Chen, S. H. Chien, K. D. Closser, D. L. Crittenden, M. Diedenhofen, R. A. DiStasio, H. Do, A. D. Dutoi, R. G. Edgar, S. Fatehi, L. Fusti-Molnar, A. Ghysels, A. Golubeva-Zadorozhnaya, J. Gomes, M. W. D. Hanson-Heine, P. H. P. Harbach, A. W. Hauser, E. G. Hohenstein, Z. C. Holden, T. Jagau, H. Ji, B. Kaduk, K. Khistyayev, J. Kim, J. Kim, R. A. King, P. Klunzinger, D. Kosenkov, T. Kowalczyk, C. M. Krauter, K. U. Lao, A. D. Laurent, K. V. Lawler, S. V. Levchenko and C. Y. Lin, *Mol. Phys.*, 2015, **113**, 184–215.
- ²³K. Raghavachari, G. W. Trucks, J. A. Pople and M. Head-Gordon, *Chem. Phys. Lett.*, 1989, **157**, 479–483.
- ²⁴A. L. L. East and W. D. Allen, *J. Chem. Phys.*, 1993, **99**, 4638–4650.
- ²⁵A. Halkier, T. Helgaker, P. Jørgensen, W. Klopper, H. Koch, J. Olsen and A. K. Wilson, *Chem. Phys. Lett.*, 1998, **286**, 243–252.
- ²⁶A. E. DePrince and C. D. Sherrill, *J. Chem. Theory Comput.*, 2013, **9**, 2687–2696.
- ²⁷M. Nishio, M. Hirota and Y. Umezawa, *The CH/π Interaction*, Wiley-VCH, New York, 1998.
- ²⁸E. H. Krenske and K. N. Houk, *Acc. Chem. Res.*, 2013, **46**, 979–989.
- ²⁹A. L. Ringer, M. S. Figgs, M. O. Sinnokrot and C. D. Sherrill, *J. Phys. Chem. A*, 2006, **110**, 10822–10828.

Isomer	Conf.	CCSD(T)/CBS			B3LYP-D3/TZVP			Experiment
		ΔE_{gas}	$\Delta\Delta G_{\text{solv}}$	% Pop.	ΔE_{solv}	$\Delta\Delta G_{\text{solv}}$	% Pop.	% Pop.
<i>(S,R) anti</i>	1	0.00	0.00	98.81	0.00	0.00	99.30	45-47
	2	0.45	0.15		0.25	-0.05		
	3	2.77	3.45		1.47	2.15		
	4	2.58	3.33		1.07	1.82		
<i>(S,S) syn</i>	1	1.37	2.79	0.98	1.57	2.99	0.68	43-45
	2	1.65	2.84		1.73	2.92		
	3	3.35	5.38		2.70	4.73		
	4	2.81	5.07		1.96	4.22		
<i>(R,R) ent-syn</i>	1	7.42	9.18	0.00	5.24	7.00	0.01	5-7
	2	5.01	6.91		3.19	5.09		
	3	8.05	9.72		5.87	7.54		
	4	6.45	8.03		4.30	5.88		
<i>(R,S) ent-anti</i>	1	6.26	5.84	0.21	7.51	7.09	0.01	3-5
	2	3.37	3.35		5.35	5.33		
	3	8.13	7.60		8.36	7.83		
	4	5.57	4.90		6.43	5.76		

TABLE I. The relative total energies of the transition states (ΔE), relative Gibbs free energies at 298K ($\Delta\Delta G$), and percent populations are listed for the CCSD(T)/CBS estimates obtained in this work and the previous best estimate by Rzepa and co-workers⁴ at the B3LYP-D3/TZVP/SCRF=DMSO level of theory. CCSD(T)/CBS ($\Delta\Delta G$) results include solvent and thermodynamic corrections obtained at the B3LYP-D3/TZVP/SCRF=DMSO level. Experimentally measured³ product ratios are presented for comparison. All energetics are reported in kcal mol⁻¹ and evaluated at the B3LYP-D3/TZVP/SCRF=DMSO geometries of Rzepa and co-workers.⁴

CCSD(T)/CBS				
Isomer	Conf.	Interaction Energy	Deformation Energy	O-H Bond Length
<i>(S,R) anti</i>	1	-44.51	47.57	1.25
	2	-45.32	48.85	1.25
	3	-51.22	57.04	1.31
	4	-52.30	57.95	1.31
<i>(S,S) syn</i>	1	-50.81	55.27	1.29
	2	-51.09	55.83	1.28
	3	-59.27	65.68	1.36
	4	-60.02	65.90	1.36
<i>(R,R) ent-syn</i>	1	-61.12	71.59	1.36
	2	-60.78	68.85	1.36
	3	-68.85	79.91	1.39
	4	-69.34	78.81	1.39
<i>(R,S) ent-anti</i>	1	-38.26	47.63	1.17
	2	-36.86	43.30	1.14
	3	-42.45	53.66	1.25
	4	-40.98	49.65	1.22
Enamine Intermediate				0.98

TABLE II. The total interaction energies and deformation energies at the CCSD(T)/CBS level of theory (kcal mol^{-1}), and carboxylic acid O-H bond length (\AA) for each transition state. Energies evaluated at the B3LYP-D3/TZVP/SCRF=DMSO transition state geometries of Rzepa and co-workers.⁴